Desalination and Water Treatment
www.deswater.com
doi: 10.5004/dwt.2023.29954

310 (2023) 167–180
October

Equilibrium, kinetics, and thermodynamics study of phenol adsorption onto *Phoenix dactylifera* leaf adsorbents

Abderrahim Khelfaoui[a,*], Noura Chaouch[b]

[a]*Process Engineering Department, Faculty of Applied Sciences, Kasdi Merbah University, 30000 Ouargla, Algeria, Tel.: +213671362328; email: khe_rahim@yahoo.com*
[b]*Process Engineering Laboratory, Process Engineering Department, Faculty of Applied Sciences, Kasdi Merbah University, 30000 Ouargla, Algeria, Tel.: +213776657101; Fax: +213 29 711975; email: amirchaouch@gmail.com*

Received 28 May 2023; Accepted 5 September 2023

ABSTRACT

Phenol is known to be toxic pollutant causing adverse impact on human health and environment. Thus, the present study aimed to remove the phenol from aqueous solutions utilising natural palm date natural leaf (NL) and palm date leaf chemically activated with H_3PO_4 activated carbon leaf (ACL). Brunauer–Emmett–Teller analysis, Fourier-transform infrared, X-ray diffraction, and scanning electron microscopy coupled with energy-dispersive X-ray spectroscopy are techniques used to characterize the sorbents. The phenol removal capacity of NL and ACL was investigated in batch experiments taking phenol content (10–70 mg/L), time (15–240 min), pH (2–12), adsorbent dose (0.1–0.6 g), and temperature (25°C–65°C). The maximum decontamination efficiencies of (42.4%) and (91.5%) on NL and ACL, respectively, were obtained at a pH of 6, temperature 25°C and adsorbent dose of 0.4 g for each. The kinetic and equilibrium adsorption data of phenol fit well to the pseudo-second-order model and Temkin isotherm, respectively. Furthermore, the utmost phenol sorption capacity of 7.645 and 13.369 mg/g was attained for NL and ACL, respectively. The results of studied diffusion models revealed that the mechanism of phenol adsorption onto NL and ACL was not only controlled by film diffusion but also by intraparticle diffusion. Also, a thermodynamic study identified the non-spontaneous and exothermic nature of adsorption. The research determined that NL and ACL could be promising and potential adsorbents for the removal of phenol from contaminated water.

Keywords: Adsorption models; Phenol; Activated carbon; Thermodynamics; Kinetics

1. Introduction

Clean water supply is an important issue that has recently received considerable attention. Humen activities frequently produce effluents containing various contaminants and spread them into the environment [1]. Among the different contaminants, phenol and its derivatives belong to organic compounds and are commonly distributed in the environment including wastewater due to many industries like the chemical industry (facilities of production of some derivatives such as alkylphenols, cresols), petrochemical, coking, plastics, paper and refineries, pesticides paints, fertilizers, surfactants, and pharmaceutical [2,3].

Poor biodegradability and solubility, long term ecological harm and high toxicity of phenol and its derivatives led to being classified by the Environmental Protection Agency (EPA) as pollutants of priority concern and there concentrations should not exceed the limit values of water discharge. For example, the permissible level of phenol in the wastewater is restricted to 1 mg/mL [4,5].

To ensure the safe limits of phenol in aqueous streams, many technologies have been used for phenol removal from wastewaters, such as membrane separation [3],

* Corresponding author.

coagulation–flocculation [6], advanced oxidation [7], biological treatments [8], ion exchange [9], and adsorption [10]. Among them, the adsorption process has been extensively used for the removal of organic compounds in aqueous solutions because of its ease of operation and control, extensive compatibility, low operational costs, high efficiency and, additionally, the possibility to regenerate which allows the reuse of adsorbents and phenol recoveries for further purposes [11,12].

Clays, polymers, zeolites, surfactant-modified zeolites, carbon nanotubes, fly ash, and activated carbon are some of the absorbents used for phenol removal [13]. Lately, significant consideration has been directed towards low-cost and the most efficient adsorbents. Thus, activated carbons prepared from by-products of agriculture and industries are the most widely used and could be assumed to be low-cost adsorbents since their starting materials are abundant, inexpensive, and require little processing [14]. Several studies have been carried out on phenol removal by activated carbon developed from agriculture by-products like sawdust, rice husk, bark, rubber seed coat, apricot stone shells, and corncob [14,15].

Phoenix dactylifera, commonly known as the date palm belongs to the family Arecaceae [16,17]. It is the most significant agricultural crop, found abundantly in south of Algeria. Palm date waste is considered a great burden on farms and date canning factories. They form observable environmental pollution from the accumulation of palm tree residues: leaves, fronds, worn trunks, and seeds. Some studies have proved that one date palm can generate about 20 kg of waste per year, which prompted the need to find alternatives to create transformational projects for these by-products [17]. Therefore, the conversion of these wastes into activated carbon production for the removal of organic pollutants from aqueous solutions is a right step in the right direction and of great importance from an environmental and economic point of view [18].

Thus, the aim of present work was to investigate the adsorption performance of phenol from an aqueous solution using naturel leaf and activated carbon leaf of *Phoenix dactylifera* as inexpensive adsorbents. The effect of different experimental variables on the adsorption process was studied, including pH solution, contact time, initial phenol concentration, amount of adsorbent, and temperature. Equilibrium models, kinetic studies, and thermodynamic aspects were also investigated.

1.1. Reagents and solutions

Hydrochloric acid (HCl, 99%), sodium chloride (NaCl, 99%), phosphoric acid (H_3PO_4, 85%), and (phenol 99.8%) were purchased from Sigma-Aldrich (St. Louis, Missouri, USA). A stock solution containing 1,000 mg/mL of phenol was prepared dissolving an appropriate amount in bi distilled water. Desired concentrations of working solutions were achieved by adequate dilution of stock solution.

2. Materials and methods

2.1. Preparation of adsorbents

2.1.1. Adsorbent natural leaf

The leaves were collected from Ouargla's oases (latitude and longitude coordinates are: 31° 57′ 9.6192″ N, 5° 20′ 0.6864″ E), southeast of Algeria and washed with water to remove impurities. The leaves obtained were cut into small pieces and washed again with distilled water, then dried in an oven overnight for crushing and sieving to desired particle size.

2.1.2. Adsorbent activated carbon leaf

The activated carbon leaf (ACL) was prepared by immersing of 50 g of natural leaf (NL) in 500 mL of phosphoric acid solution (30% acid + 70 bi-distilled water) at 60°C for an entire day using rotary incubator shaker. The mixture was filtered and dried in the oven for 24 h. The dried material was carbonized at 450°C for about 1.5 h in muffle furnace. Finally, the activated carbon obtained was washed with distilled water and dried for 24 h in an oven at 105°C. The adsorbents were stored in closed containers for different uses.

2.2. Characterisation equipment

In this study, nitrogen adsorption measurements were conducted with a Micromeritics 3Flex adsorption analyser (Norcross, Georgia, USA). The infrared (IR) spectra were recorded by (Cary 640 Fourier-transform infrared spectrometer (FTIR) of Agilent Technologies, Santa Clara, California, USA) using pellets of KBr accessory. BTX III X-ray diffraction (XRD) analyzer with CuKa radiation (λ = 1,5418 A°) was used for X-ray diffraction (XRD) measurement. The scanning electron microscopy instrument (JEOL JSM-7600F, Akishima, Tokyo, Japan) was used for scanning electron microscopy (SEM) images of the sorbents at different magnifications. The SEM was coupled with an energy-dispersive X-ray spectroscopy (EDS) in order to provide elemental and chemical analysis of the samples.

2.3. Adsorption studies

Batch adsorption experiments (Table 1) were conducted to study the effect of five adsorption parameters namely pH solution, contact time, adsorbent dosage, initial concentration, and temperature on phenol removal efficiency. All adsorption experiments were carried out in 250 mL Erlenmeyer flasks containing 20 mL of phenol solution kept in the incubator shaker at 300 rpm for each batch run.

The solid/liquid mixture was filtered using Grade 1 Whatman filter paper (pore size 11 μm). Analysis of residual phenol in the aqueous phase was determined by a UV-visible spectrophotometer (UV-DR 6000) at the wavelength (λ_{max} = 270 nm). Each experiment was performed twice, and the average results are presented in this study.

The adsorption capacity (q_e) (mg/g) and the percentage removal of phenol (PR) at equilibrium were calculated using Eqs. (1) and (2):

$$q_e = \frac{C_0 - C_e}{m} V \tag{1}$$

$$\mathrm{PR}(\%) = \frac{C_0 - C_e}{C_0} \times 100 \tag{2}$$

where C_0 and C_e are initial and equilibrium phenol concentrations (mg/L), respectively. V is the volume of solution (L) and m is the mass of the adsorbent (g).

3. Results and discussions

3.1. Characterization of CN and ACF

3.1.1. Textural characterization

Fig. 2 shows the nitrogen adsorption–desorption isotherm and pore size distribution of the samples. We can see that the adsorption/desorption curves of the samples present differently but both NL and ACL exhibit hysteresis loops (the desorption is not coexistent with the adsorption isotherm), which indicate the presence of mesopores in the samples. According to the classification of gas adsorption isotherms defined by the International Union of Pure and Applied Chemistry (IUPAC), the isothermal curve of NL could be classified as intermediate between types II and IV, indicating a nonporous structure with fewer mesopores, while ACL showed mixed characteristics of types I and IV, indicating that the sample developed a certain amount of micro and mesopores. Moreover, the big deviation between sorption curves led to open hysteresis (for ACL), which has already been observed in many previous studies. However, the reason for this phenomena may due to deformation of micro-structures of carbonaceous materials, especially during low temperature N_2 sorption [19].

Fig. 2 (insets) also shows Barrett–Joyner–Halenda (BJH) pore size distributions, ranging from 1.93 to 33.70 nm and 1.97 to 44.36 nm for NL and ACL, respectively, confirming the existence of micropores (<2.0 nm) and mesopores (2.0–50.0 nm) according to the BJH adsorption pore distribution. Additionally, the cumulative pore volume of ACL is

Table 1
Summarizes for all experiments of batch adsorption

Investigation	pH	Time (min)	Adsorbent dosage (g)	Initial phenol concentration (mg/L)	Temperature (°C)
Effect of pH	2, 4, 6, 8, 10, and 12	120	0.1	50	25
Effect of time	Optimum pH	15, 30, 60, 90, 120, 150, 180, 210, and 240	0.1	50	25
Effect of sorbent dosage	Optimum pH	120	0.1, 0.2, 0.3, 0.4, 0.5, and 0.6	50	25
Effect of initial phenol concentration	Optimum pH	120	0.1	10, 20, 30, 40, 50, 60, and 70	25
Effect of Temperature	Optimum pH	120	0.1	50	25, 35, 45, 55, and 65

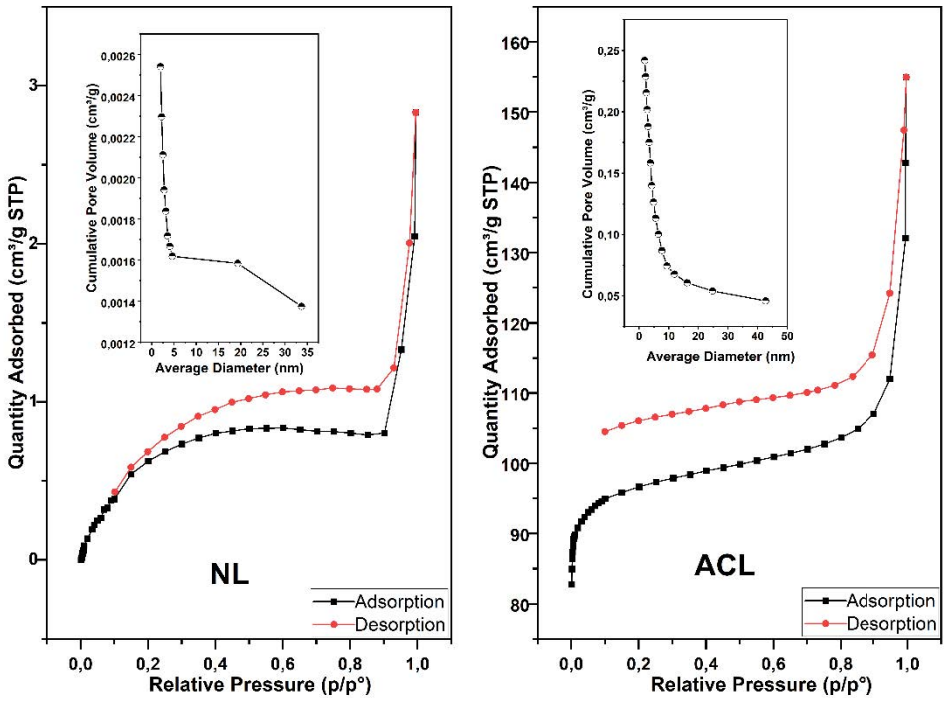

Fig. 1. Nitrogen adsorption/desorption isotherms and the corresponding pore size distributions (insets) of natural leaf and activated carbon leaf.

0.241 cm^3/g, 95 times larger than that of NL (0.00254 cm^3/g); this is due to more pores contained in ACL compared with the raw sample. These findings corresponded to the results listed in Table 2, which summarizes the physical properties of the adsorbents.

Based on Table 2, it can be observed that the Brunauer–Emmett–Teller (BET) surface area and pore volume of NL are less than those of ACL. The process of activation with phosphoric acid and carbonization clearly yielded a high surface area and porosity [20]. It can also be noted that most pores represent the mesoporous structure according to the values of the average pore size of samples.

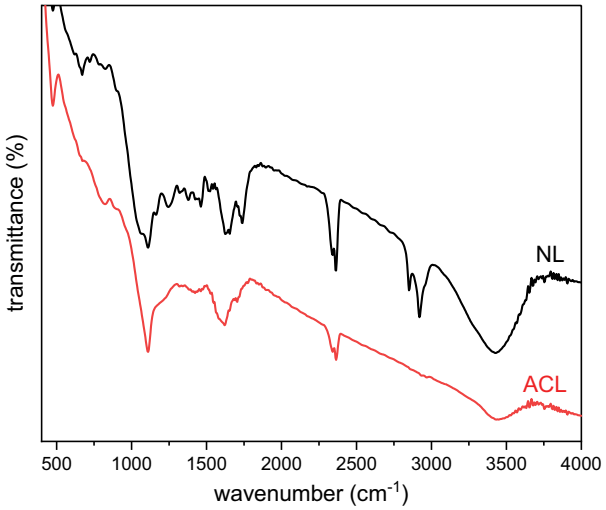

Fig. 2. FTIR spectra of natural leaf and activated carbon leaf.

3.1.2. Infrared spectroscopy

FTIR analysis was conducted in order to identify the functional groups on samples surfaces. FTIR spectrum of raw material and activated carbon are presented in Fig. 2. Based on this figure, the characteristic adsorption peaks of the NL and ACL were different. The intensity of some peaks decreased like the broad peak at 3,428 cm^{-1} which belongs to the stretching vibration of the hydroxyl (O–H) or the water molecule adsorbed by sorbents. This observation was also supported by peak at 1,654 cm^{-1}. The reduction in intensity means a decreasing in amount of hydrogen and an increase in amount of carbon and this was proved by the results of elemental analysis [21].

In addition, some peaks disappeared in ACL relative to the NL as many of the functional groups disappeared after the activation processes and this applied to minor peaks between 1,461 to 1,172 cm^{-1}. This result is due to the thermal degradation effect during carbonization which led to destruction of some intermolecular bonding [22]. Table 3 summarizes the FTIR peaks and assigned functional groups.

3.1.3. X-ray diffraction

The crystalline behaviour of NL and ACL were investigated by XRD and outcomes are exhibited in Fig. 3. X-ray diffraction spectra suggested the presence of crystalline and amorphous regions. The crystalline order which belongs to

Table 2
Textural characteristics of NL and ACL

Sample	S_{BET} [a] (m^2/g)	S_{ext} [b] (m^2/g)	S_{mic} [c] (m^2/g)	V_p [d] (cm^3/g)	V_{mic} [e] (cm^3/g)	D_{BET} [f] (nm)
NL	1.731	1.731	nd	0.00234	nd	5.406
ACL	306.338	86.824	219.513	0.165	0.108	2.159

[a]Surface area calculated from BET method;
[b,c,e]are derived using *t*-plot method;
[d]Pore volume deduced from single point adsorption method at $P/P_0 = 0.995$;
[f]Calculated using $4V_p/S_{BET}$;
nd: not detected.

Table 3
FTIR peaks and corresponding functional groups

Wavelength (cm^{-1})	Functional group	Molecules responsible
3,428	Stretching vibrations of O–H bonds	Cellulose, hemicelluloses, lignin or water molecule because of moisture content
2,923–2,861	Stretching vibration of C–H bond (asymmetrical and symmetrical) in alkyl groups	Cellulose, lignin, and hemicellulose
2,368	C–O stretching	May due to presence of atmospheric CO_2
1,743–1,704	C=O stretching vibrations in various carbonyl groups	Lignin and hemicellulose
1,654–1,623	Stretching vibrations of aromatic C=C bonds	Lignin
1,461–1,176	Stretching vibrations of C–O, C–H, and CH_2 bending of aliphatic and aromatic CO groups and O–H in plane bending	Hemicelluloses, cellulose, pectin
1,114–1,110	Antisymmetric stretching of –C–O–C–	Cellulose

cellulose is evident in samples by three peaks near 2θ~14.15, 2θ~17.1, and 2θ~21.25 [23]. Furthermore, the results showed a decrease in amorphous components, which led to a slight increment in crystallinity of ACL compared with NL. The exclusion of amorphous hemicellulose and lignin occurred by preferential pyrolysis with H_3PO_4 during chemical activation or exposure to high temperature during calcination [23–25]. Generally, the thermal degradation temperature of cellulose is mainly in the range of 100°C–400°C [25]. However, cellulose was not affected by temperature of 450°C and this may due to its high crystallinity degree which led to its resistance to thermal decomposition [26].

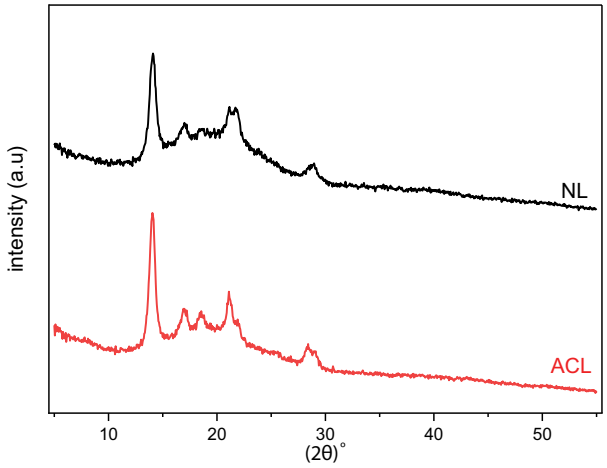

Fig. 3. XRD diffractograms of natural leaf and activated carbon leaf.

3.1.4. SEM and elemental analysis

Fig. 4 shows SEM images and EDX spectra of NL and ACL. As observed, both adsorbents had an irregular shape. The surface of NL was relatively smooth, poreless, and unified without cavities or cracks, indicating the presence of cellulose, hemicelluloses, and lignin in the raw material [27]. In contrast, cavities and pores were clear for ACL. This have been caused by removal of volatile matter after chemical activation and pyrolysis at 450°C [28]. Previous studies have proved that surface porosity and pores volume were increased after carbonization process, resulting a large surface area [27,28].

The EDS analysis revealed the presence of three elements (C, O, and Si) in both sorbents. It was found that the carbon content increased while the oxygen element decreased. This could be due to the decomposition of biomass and carbonization in addition to volatilization process in NL during the pyrolysis [27,29]. A small O/C ratio

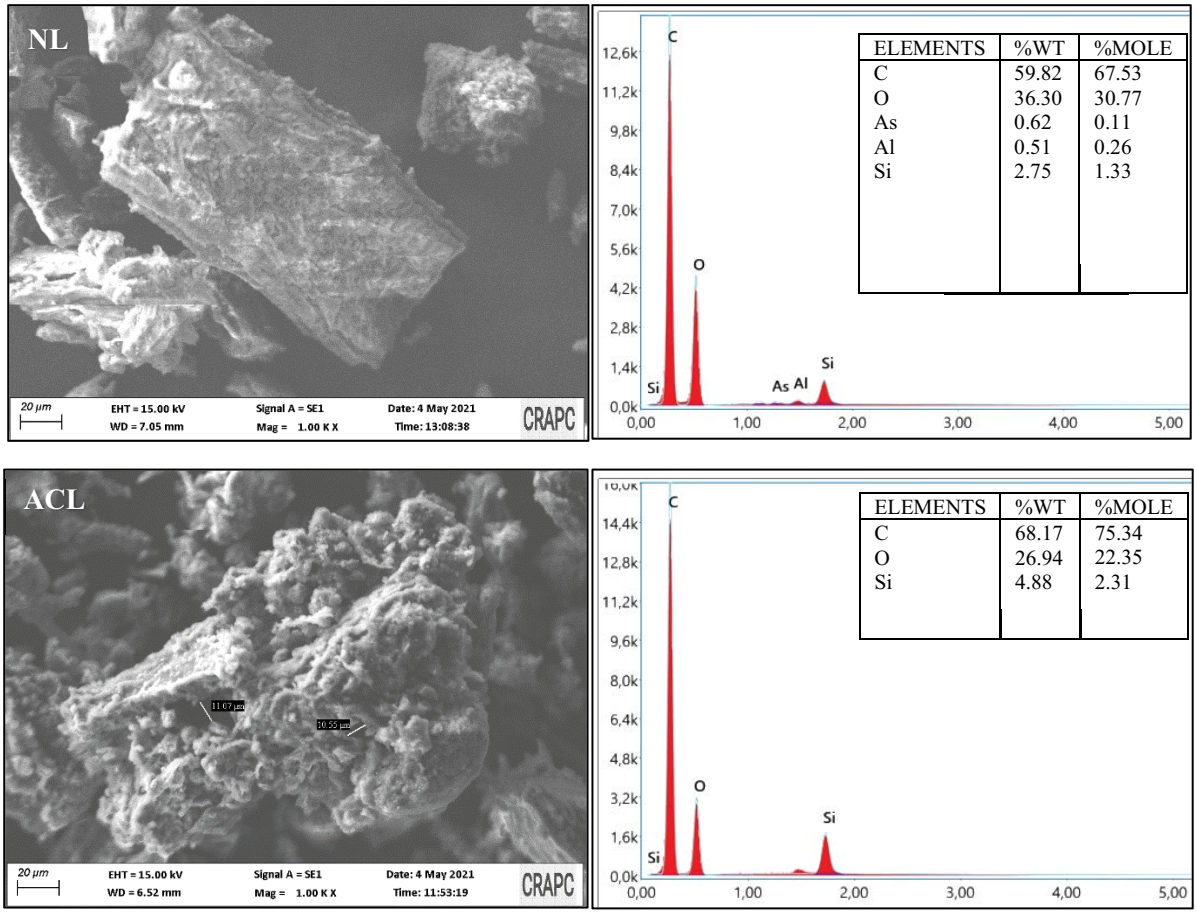

Fig. 4. SEM-EDS analysis of natural leaf and activated carbon leaf.

means that resulting activated carbon consists mainly of fixed carbon aromatic rings and is thus chemically stable [30]. The presence of Si could be attributed to diode probe of apparatus. The EDS analysis also showed an absence of phosphorus (P) in the activated carbon, this was evidence of the washing effectiveness.

3.2. Effect of adsorption parameters

3.2.1. Effect of pH

pH of the adsorption medium plays a very important role in the adsorption process. It has a strong influence on surface charge of the adsorbent and the ionisation degree of the adsorbate. It can be seen from Fig. 5a that the rate of the removal of phenol on NL and ACL increases with the increase in pH (up to pH = 6) then decrease after this point. The optimum adsorption capacities onto NL and ACL take place in pH of 6 with the maximum percentage removal of 32% and 67.63%, respectively.

Mechanism can be elaborated on the basis of ionisation of solution and surface charge of the adsorbents. However, at high pH values (pH > phenol pKa [9.89]), the percentage removals decrease due to ionization of phenol and electrostatic repulsion force between negative adsorbents sites and negative phenolate ions ($C_6H_5O^-$). While at pH < phenol pKa the percentage removal is higher because phenol is in molecular form and the dispersion interaction predominated [15,31]. Effect of pH on batch adsorption studies of phenol by activated biochar derived from cow-dung [32] and corn husk derived magnetized activated carbon [33] indicated that phenol was better adsorbed at pH = 6.

3.2.2. Effect of contact time

The results of contact time effect on adsorption efficiency are presented in Fig. 5b. The studies revealed a rapid increase in phenol removal within the first 15 min which was due to concentration gradient between adsorbate and adsorbent in the solution as well as the active binding sites availability [34]. The slow phase in the adsorption process could be due to competition between the adsorbate molecules for the remaining vacant surface sites or repulsive forces between the solute molecules in the solid and solution phases [34,35]. Thus, the equilibrium time for the adsorption of phenol was reached at 150 and 180 min for NL and ACL, respectively. NL took less time than ACL because it had fewer active sites.

3.3. Effect of adsorbent dose

Fig. 5c presents the effect of Adsorbent dose. The result showed that the percentage removal raised by increasing the adsorbent dose with maximum phenol removal of 42.4% and 91.5% for NL and ACL, respectively. This phenomenon

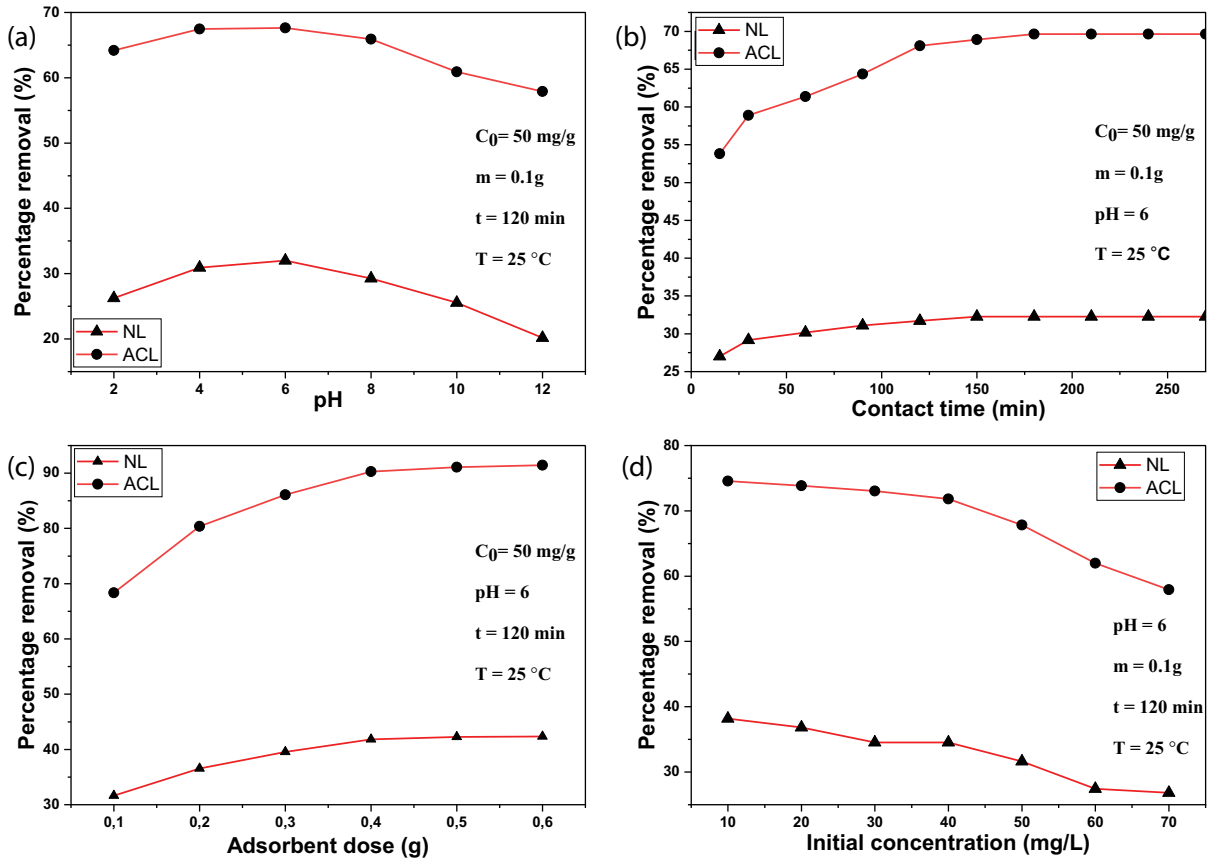

Fig. 5. Effect of pH (a), contact time (b), adsorbent dose (c) and initial concentration (d) on phenol adsorption onto natural leaf and activated carbon leaf.

could be explained by availability of more adsorption sites with increase in adsorbent dosage which resulted high phenol adsorption efficiency [36]. It was also observed that the optimum dose for both adsorbents is 0.4 g because there was no significant increase in the adsorption after this value. Despite the increase in the number of active sites (adsorbent dose), the adsorption process has become more difficult, and this might be due to overlapping or aggregation of adsorption sites [34].

3.3.1. Effect of initial concentrations

The effect of initial concentration of phenol on the adsorption are shown in Fig. 5d. By increasing the initial phenol concentration from 10 to 70 mg/L, the percentage removals were decreased from 38.18% to 26.81% for NL and 74.54% to 57.92% for ACL. However, the adsorption capacities were increased from 0.76 to 3.75 mg/g and 1.49 to 8.10 mg/g for NL and ACL, respectively. At high concentration, due to availability of vacant surface sites during the initial stage and to adsorbent weak resistances to mass transfer of phenol, high adsorption capacities were observed. While low percentage values were noticed due to the excess amount of phenol with lack of available active sites on the adsorbents surfaces as time increased [37]. Similar results have been reported in the literature [10].

3.3.2. Equilibrium modelling

Adsorption isotherms explain the equilibrium relationships between adsorbed phenol and adsorbent. In this work, Langmuir, Freundlich, Temkin, and Dubinin–Radushkevich isotherms were used to study the behaviour and mechanism of the adsorption for phenol on NL and ACL.

The Langmuir model assumes that adsorption occurs at specific homogeneous sites via monolayer adsorption without interaction between adsorbed molecules [38]. The linear form of Langmuir model is represented in Eq. (3). Where q_m is the maximum adsorption capacity (mg/g) and K_L is the Langmuir isotherm constant (L/mg).

$$\frac{C_e}{q_e} = \frac{1}{q_m K_L} + \frac{C_e}{q_m} \tag{3}$$

The separation factor R_L is a dimensionless constant can be calculated by Eq. (4):

$$R_L = \frac{1}{1 + C_0 K_L} \tag{4}$$

where R_L values indicate the adsorption to be either unfavourable ($R_L > 1$), linear ($R_L = 1$), favourable ($0 < R_L < 1$), or irreversible ($R_L = 0$).

Freundlich isotherm model is used to describe the multilayer adsorption with interaction between adsorbed molecules on heterogeneous surfaces [39]. The linear form of this model can be represented by Eq. (5):

$$\ln q_e = \ln K_F + \left(\frac{1}{n}\right) \ln C_e \tag{5}$$

where K_F is the constant relevant to the relative adsorption capacity of the adsorbent (mg/g) and $1/n$ is the adsorption intensity.

The Temkin isotherm model is based on the assumption of the heat of adsorption of all molecules decreases linearly with the increase in coverage of the adsorbent surface taking into account the adsorbate–adsorbent interaction [40]. The linear form of Temkin isotherm is expressed as:

$$q_e = \frac{RT}{b_T} \ln K_T + \frac{RT}{b_T} \ln C_e \tag{6}$$

where T is absolute temperature (K), R is the universal gas constant (8.314 J/mol·K), K_T and b_T are Temkin isotherm equilibrium binding constant (L/g) and the Temkin constant related to the adsorption heat (J/mol), respectively.

Dubinin–Radushkevich isotherm is generally used to confirm that the adsorption was chemisorption or physisorption and also to account for the effect of the porous structure of the adsorbents [41,42]. The linear form of Dubinin–Radushkevich isotherm is:

$$\ln q_e = \ln q_m - \beta \varepsilon^2 \tag{7}$$

where β is Dubinin–Radushkevich isotherm constant (mol^2/kJ^2) and ε is the Polanyi potential, corresponding to:

$$\varepsilon = RT \ln\left(1 + \frac{1}{C_e}\right) \tag{8}$$

The mean free adsorption energy (kJ/mol) as shown by the following relationship:

$$E = \frac{1}{\sqrt{2\beta}} \tag{9}$$

Outcomes for the equilibrium isotherm studies are given in Table 4 and plots are shown in Fig. 6. From the results, it was concluded that the equilibrium data fitted more with Temkin compared with Langmuir, Freundlich and D-R isotherms. The higher correlation coefficient values ($R^2 = 0.9811$ and 0.9899 for NL and ACL, respectively) for Temkin indicated the uniformity distribution of binding energies at the adsorbent surfaces. The obtained values of b_T were 1.731 and 0.876 kJ/mol for NL and ACL, respectively at 25°C, indicating that the adsorbate–adsorbent interaction had physical nature. This supposition was confirmed by the values of the mean free energy from the D-R isotherm model that were predicted to be 0.224 and 0.5 kJ/mol for NL and ACL, respectively [43]. The positive sign for b_T illustrated that adsorption process was exothermic on NL and ACL [44].

The calculated R_L values from the Langmuir model, which were in between 0 and 1, indicated the favourable adsorption of phenol onto both adsorbents. The obtained n values from the Freundlich isotherm were between 1 and 10, which means the adsorbents were suitable for adsorption [45]. Ho and Adnan [46] demonstrate that adsorption of phenol by using coconut shell activated carbon was better represented by the Temkin model.

Table 5 shows a comparison of q_m values from Langmuir model in this study with the phenol maximum adsorption capacities onto several adsorbents.

Table 4
Isotherm parameters for phenol adsorption onto NL and ACL

Isotherm	Parameters	NL	ACL
Langmuir	q_m (mg/g)	7.645	13.369
	K_L (L/mg)	0.0191	0.057
	R_L	0.512	0.26
	R^2	0.9453	0.9622
Freundlich	K_F (L/g)	0.212	0.914
	n	1.333	1.444
	R^2	0.9783	0.9538
Temkin	K_T (L/g)	0.248	0.62
	b_T (kJ/mol)	1.731	0.876
	B	1.431	2.829
	R^2	0.9811	0.9899
Isotherm (D-R)	q_m (mg/g)	3.029	6.559
	β (mol²/J²)	10^{-5}	2×10^{-6}
	E (kJ/mol)	0.224	0.500
	R^2	0.8679	0.8815

3.4. Kinetic study

Kinetic study was performed in order to predict the sorption mechanism of phenol onto NL and ACL.

Table 5
Comparison of maximum adsorption capacities of phenol by various adsorbents

Adsorbent	q_{max} (mg/g)	References
NL	7.645	This study
ACL	13.369	This study
Vegetal cords	6.21	[47]
GO-PNIPAM	12.742	[48]
Tea waste	7.503	[49]
Nanocomposite	5.82	[50]
Coconut shell activated carbon	19.02	[46]
Luffa cylindrica fibers	9.25	[51]
Kaolinite	1.71	[52]
Metakaolinite	5.82	[52]
Corn husk activated carbon (CHAC-250)	6.468	[33]
Corn husk activated carbon (CHAC-500)	8.445	[33]
Clarified sludge	1.053	[53]

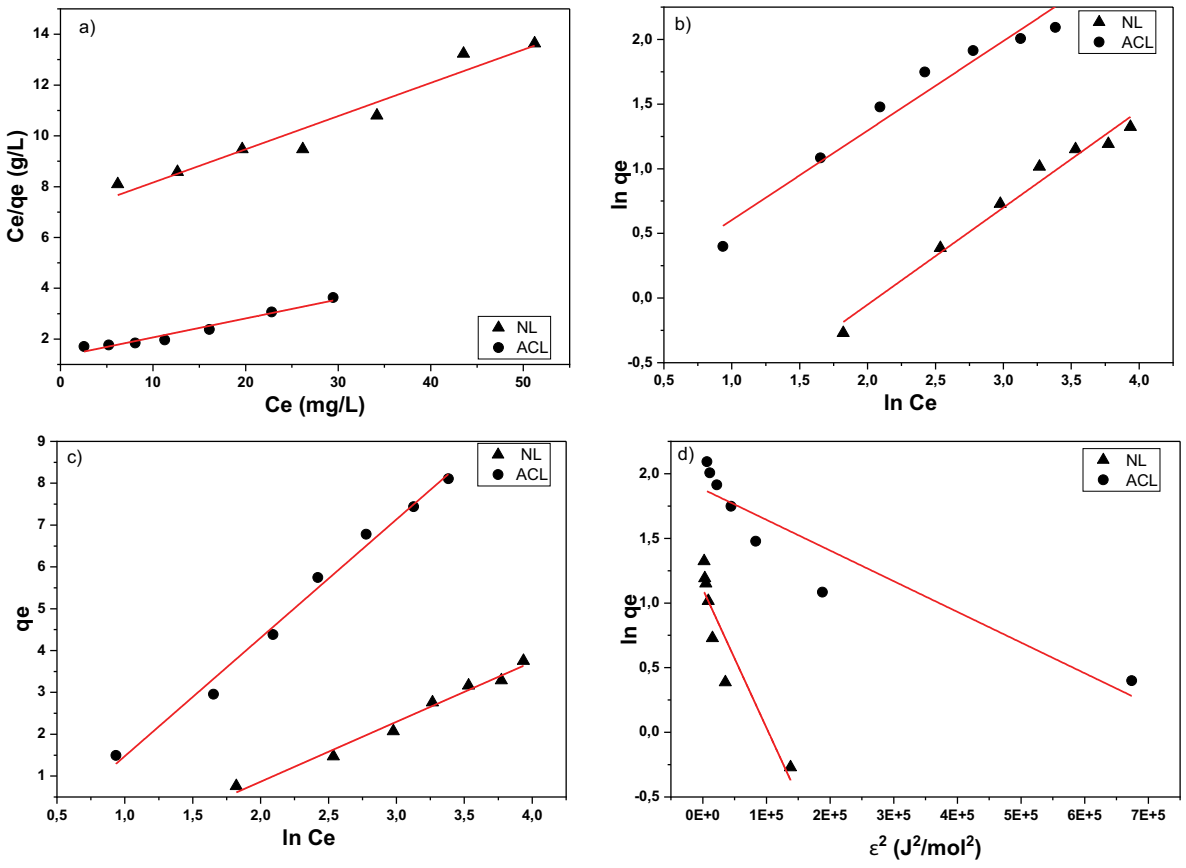

Fig. 6. (a) Langmuir plot, (b) Freundlich plot, (c) Temkin plot and (d) Dubinin–Radushkevich plot for phenol adsorption by natural leaf and activated carbon leaf.

Pseudo-first-order, pseudo-second-order, and Elovich kinetic models were applied to fit the experimental data. The linear form of pseudo-first-order, pseudo-second-order, and Elovich models are described by following Eqs. (10)–(12), respectively:

$$\ln\left(q_e - q_t\right) = \ln q_e - K_1 \cdot t \tag{10}$$

$$\frac{t}{q_t} = \frac{1}{K_2 \cdot q_e^2} + \frac{1}{q_e} \cdot t \tag{11}$$

$$q_t = \frac{1}{b_e}\ln\left(a_e b_e\right) + \frac{1}{b_e}\ln\left(t\right) \tag{12}$$

where q_e (mg/g) and q_t (mg/g) are the amount of phenol adsorbed at equilibrium at time t (min), respectively; K_1 (min^{-1}) and K_2 (g/mg·min) are the adsorption rate constant of pseudo-first-order model and the adsorption rate constant of the pseudo-second-order, respectively. a_e is the initial adsorption rate constant (mg/g·min), and b_e (g/mg) is the desorption constant of the Elovich model.

where K_1 and q_e of the first model can be derived from the graph $\ln(q_e - q_t)$ vs. t while K_2 and q_e of the second model can be calculated by plotting t/q_t vs. t. The results of the kinetic models with corresponding R^2 are shown in Table 6 and plots are shown in Fig. 7. It could be seen that the correlation coefficient (R^2) of pseudo-second-order model was much higher than pseudo-first-order and Elovich. Also, the adsorption capacity (q_e) obtained at equilibrium experimentally was closer to the value obtained from pseudo-second-order model compared with pseudo-first-order kinetic model value, which suggests that the adsorption of phenol onto NL and ACL followed pseudo-second-order kinetic model. Based on pseudo-second-order postulation, adsorption process involved chemisorption mechanism [36]. Previously, adsorption of phenol from aqueous solution also presented

Table 6
Kinetic parameters of phenol removal by NL and AC

Models	Parameters	NL	ACL
Experimental	q_e exp (mg/g)	3.163	6.781
Pseudo-first-order	q_e cal (mg/g)	0.664	2.547
	K_1 (min^{-1})	0.0202	0.0224
	R^2	0.9845	0.9512
Pseudo-second-order	q_e (mg/g)	3.283	7.179
	K_2 (g/mg·min)	0.0765	0.0191
	R^2	0.9999	0.9996
Elovich	b_e (g/mg)	5.479	1,722
	a_e (mg/(g·min))	44530.356	449,023
	R^2	0.9513	0.9662

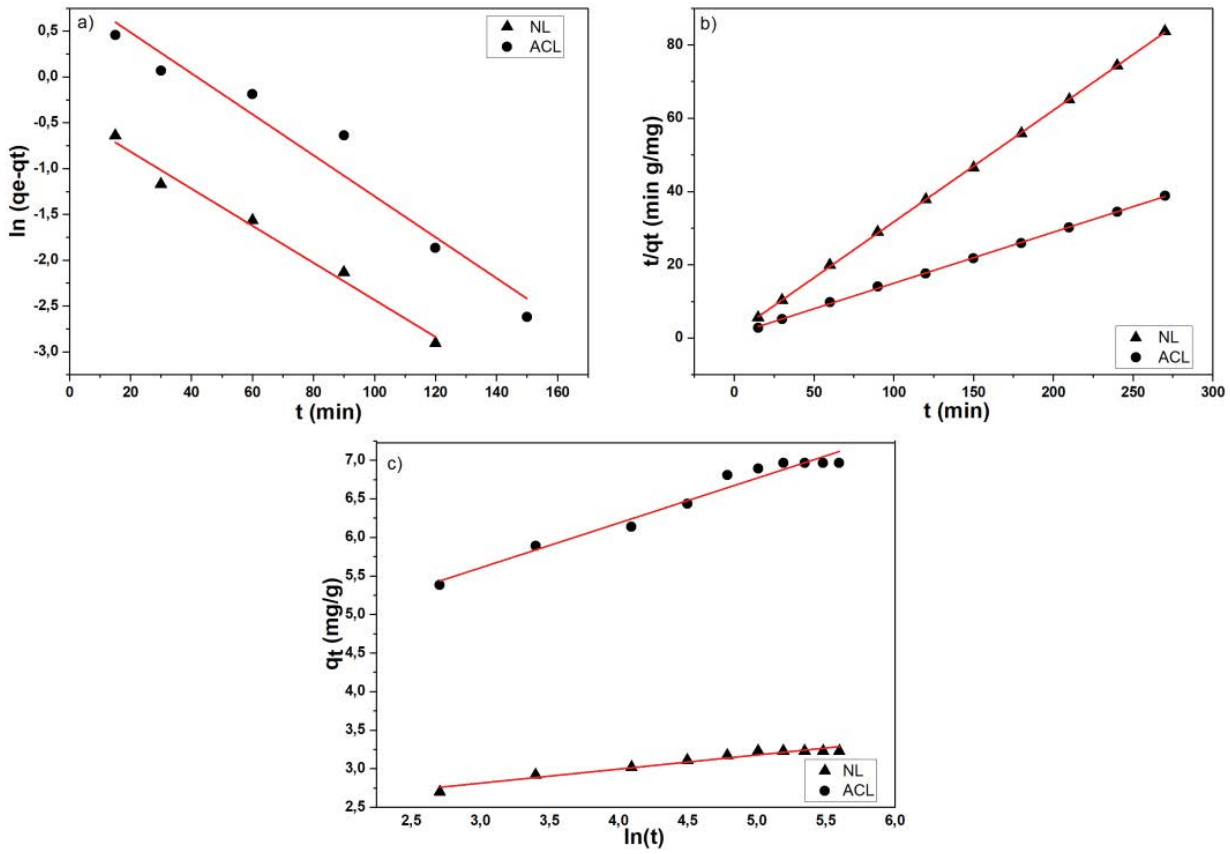

Fig. 7. Adsorption kinetic models plots for phenol adsorption onto natural leaf and activated carbon leaf (a) pseudo-first-order kinetic model, (b) pseudo-second-order kinetic model and (c) Elovich kinetic model.

a similar trend investigated by Dehmani et al. [54], El-Bery et al. [55], and Gürkan et al. [56].

3.5. Diffusion modelling

Usually, liquid adsorption process onto solid adsorbents comprises of four consecutive steps: (i) bulk diffusion, where the solute is transported from bulk solution to the liquid film surrounding the solid adsorbent; (ii) external diffusion, where diffusion of the solute takes place across the surface liquid film surrounding the solid particles; (iii) internal diffusion of the solute from the liquid film to the surface. This stage occurs via two mechanisms: (1) pore diffusion and (2) surface diffusion; (iv) solute attachment onto the active sites of the adsorbent [57–59].

The most interesting fact that the overall rate of the adsorption is controlled by the slowest step [57,58]. The first and the last steps are usually rapid compared with the second and third step [57,58,60]. Thus, first- and second-order kinetic equations cannot describe the whole adsorption process [58]. In order to understand more detailed characteristics of the adsorption process, liquid film diffusion and intraparticle models [Eqs. (12) and (13), respectively] were applied to determine the limiting step of adsorption process [59,60].

Fig. 8 represents the plots of the liquid film diffusion (LFD) and intraparticle diffusion (IPD) models. The calculated parameters are presented in Table 7. As can be seen from Fig. 8, neither a linear plot of –ln(1–F) vs. t nor a linear plot of q_t vs. $t^{0.5}$ pass through the origin indicating that the kinetics of the adsorption process was not solely controlled by intraparticle diffusion or film diffusion into both adsorbents [61]. Data points of LFD (Fig. 8a) were linearly fitted which indicated the involvement of LFD in the adsorption process of both sorbents [60]. In Fig. 8b, it is also noted that the plots represent mainly two stages of phenol adsorption. The initial linear portion represented surface adsorption (i.e., film diffusion) while second linear portion denoted intraparticle diffusion into NL and ACL [62]. The regression R^2 values (R^2 = 0.9845–0.9512 for NL and ACL, respectively) obtained from LFD model were greater than those obtained from IPD model (R^2 = 0.8443–0.8972 for NL and ACL, respectively), thus indicating the relevance of film diffusion as a rate determining factor in the adsorption process. Moreover, the larger values of the intercept C indicated the greater effect of the boundary layer on the adsorption process [57,63]. It can be concluded that the adsorption rate controlling or limiting-step of phenol in NL and ACL (i.e., the adsorption process) was predominantly controlled by film diffusion and followed by internal (intraparticle) diffusion or other processes [64]. These findings were consistent with several earlier reports [64–66].

3.6. Effect of temperature and adsorption thermodynamic study

The experimental data were used for the thermodynamic study to estimate the feasibility of phenol adsorption process on NL and ACL. The thermodynamic adsorption study was carried out at different temperatures (25°C, 35°C, 45°C, 55°C, and 65°C). The experimental conditions are the same as defined in the equilibrium experiments where the studied initial concentrations were 50 mg/L and the contact time was 120 min. Gibb's free energy change (ΔG°), enthalpy change (ΔH°), and entropy change (ΔS°) are expressed by Eqs. (13)–(16).

$$K_C = \frac{q_e}{C_e} \tag{13}$$

$$\Delta G^\circ = -RT \ln K_C \tag{14}$$

Table 7
Diffusion parameters of phenol adsorption onto NL and ACL

Models	Parameters	NL	ACL
Liquid film diffusion	K_{fd} (min^{-1})	0.0202	0.0224
	R^2	0.9845	0.9512
Intraparticle diffusion	K_{id} (mg/g·min$^{0.5}$)	0.0384	0.125
	C	2.684	5.169
	R^2	0.8443	0.8972

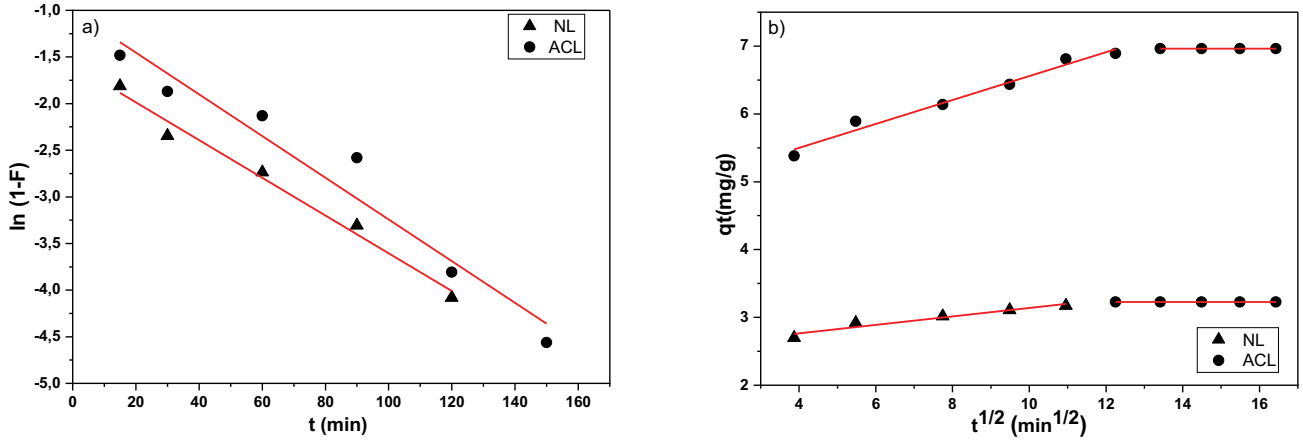

Fig. 8. (a) Liquid film diffusion plot and (b) intraparticle diffusion plot for phenol adsorption onto natural leaf and activated carbon leaf.

$$\ln K_C = \frac{\Delta S^\circ}{R} - \frac{\Delta H^\circ}{RT} \quad (15)$$

$$\Delta G^\circ = \Delta H^\circ - T\Delta S^\circ \quad (16)$$

where ΔG°, ΔH°, and ΔS° are the changes of Gibbs energy (kJ/mol), enthalpy (kJ/mol), and entropy (kJ/mol·K), while R stands for ideal gas constant (8,314 J/mol·K), and K_C is equilibrium constant (dimensionless). ΔH° and ΔS° were calculated from the slope and the intercept of the curve $\ln K_C$ of vs. $1/T$ and the values of ΔG° were calculated for the different temperatures.

The graphs in Fig. 9a shows that adsorption capacities onto NL and ACL decreased as temperature was increased. This phenomenon might be the result of a weakening of the attractive forces between adsorbent active sites and phenol when the temperature is raised. In addition to the reasons mentioned, the high temperature decreased the thickness of the boundary layer due to the increased tendency of adsorbate to escape from adsorbent surfaces to the solution phase [51,67]. According to these results, the adsorption of phenol using both adsorbents NL and ACL was an exothermic process.

The calculated thermodynamic parameters are shown in Table 8, the obtained ΔG° values were positive, suggesting that phenol adsorption process on NL and ACL were thermodynamically nonspontaneous. ΔG° values became higher as temperature became higher indicated that the adsorption became less favourable at higher temperatures [68].

The negative values of ΔH° supported the hypothesis of the exothermic nature of the process on both adsorbents, the efficiency is improved by decreasing in temperature. Moreover, ΔH° values were inferior to 40 kJ/mol, which followed a physisorption behaviour [59]. The negative values of ΔS° demonstrated a decrease in randomness at solid/solution interfaces during the adsorption process [64]. Similar results were found by Yadav et al. [69] and Khelfaoui et al. [70] who worked on the adsorption of phenol on magnetic activated carbon synthesised from cauliflower waste and on sorbent prepared from *Phoenix dactylifera* fiber, respectively.

3.7. Mechanism of phenol adsorption

The affinities of the adsorbent towards the phenol can be determined from the content of surface functional groups and the pH effects of the solution. It is also known that there are three hypotheses to interpret phenol absorption onto the adsorbents: the electron donor–acceptor complex (chemical adsorption), the π–π dispersion interactions (physical adsorption), and the solvent effects (the hydrogen-bonding formation) [71,72].

The formation of electron-donor-acceptor complex mainly appears when phenol is ionized under the experimental conditions used [73]. In this reaction, the donor and

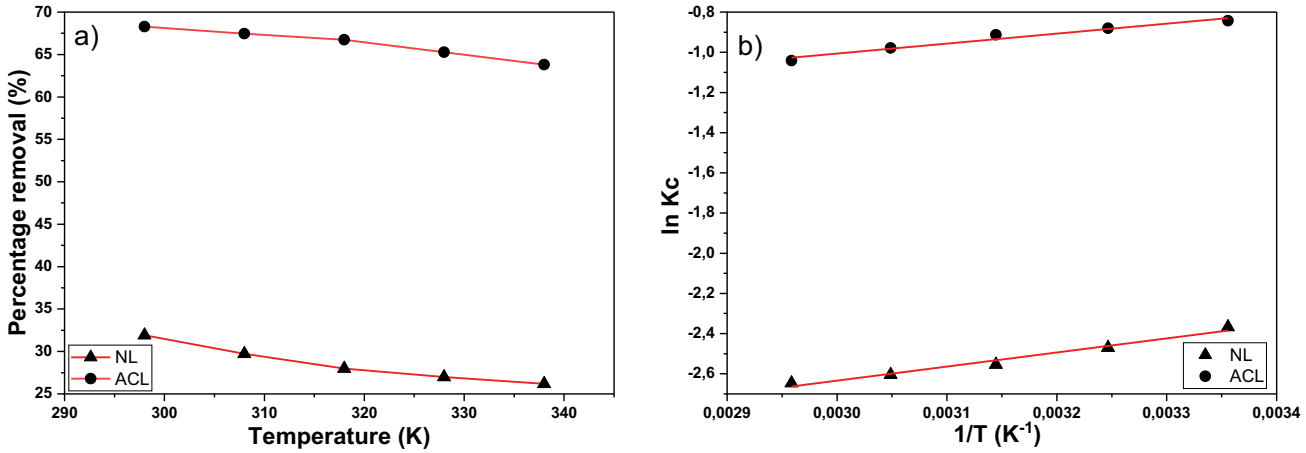

Fig. 9. (a) Effect of temperature and (b) the variation of $\ln(K_C)$ as a function of $1/T$ for phenol adsorption using natural leaf and activated carbon leaf.

Table 8
Thermodynamic parameters of phenol adsorption onto NL and ACL

Temperatures (K)	NL			ACL		
	ΔG° (kJ/mol)	ΔH° (kJ/mol)	ΔS° (kJ/mol·K)	ΔG° (kJ/mol)	ΔH° (kJ/mol)	ΔS° (kJ/mol·K)
298	5.865			2.089		
308	6.324			2.255		
318	6.752	−5.825	−0.0394	2.415	−4.124	−0.0207
328	7.101			2.668		
338	7.436			2.928		

the acceptor are the surface oxygen groups of the adsorbent and the aromatic rings of phenol [71,74], respectively. According to thermodynamic study, the phenol adsorption on NL and ACL was primarily physical, which eliminates the consideration of this mechanism as the major force.

As seen in effect of pH study, the degree of ionization phenol adsorption on both NL and ACL is lower at pH < phenol pKa and the molecular form of phenol led to an increase on its adsorption. Thus, the π–π dispersion derives from the interactions between π electrons in the aromatic rings of phenols molecules and delocalized π electrons in graphite layers are dominant [73]. Based on above-mentioned analyses, this mechanism could be considered as a main force and this was proven by thermodynamic analysis (physical adsorption).

The solvent effects take place when some active sites are occupied by water molecules rather than phenol molecules. This phenomenon occurs on the surface oxygen groups by a hydrogen bond which may block part of the pores. It is likely that one of the reasons for the difference between the experimental maximum adsorption capacity (q_e) and the monolayer adsorption capacity (q_m) [71].

It can be concluded that the adsorption of phenol on NL and AL was primarily physical (π–π dispersion interaction) with the possibility of chemical adsorption (electron donor–acceptor complex), without ignoring water effects in reducing the absorption rate.

4. Conclusion

In this present work, NL and date palm leaf chemically activated with H_3PO_4 (ACL) were successfully utilized as low-cost adsorbents for the removal of phenol from wastewater. BET analysis showed developed in textural properties, where BET surface area and pore volume of ACL larger than those obtained from NL. The chemical structure of samples was analyzed by FTIR spectroscopy. It was revealed that the adsorbents surfaces contain mainly hydroxyl and carbonyl groups. XRD results showed that NL preserved its crystalline nature after chemical activation and calcination. Moreover, SEM images showed that NL had no pores, in contrast to ACL, which had many created pores after pyrolysis process. pH = 6 and the adsorbent dose of 0.4 g offered maximum adsorption efficiencies when it arrived to 42.4% at 150 min for NL and 91.5% at 180 min for ACL. The equilibrium study demonstrated that Temkin model was more suitable to represent the experimental data in comparison to Langmuir, Freundlich and Dubinin–Radushkevich models. The q_{max} (maximum monolayer adsorption capacity) were found to be 7.645 and 13.369 mg/g for NL and ACL, respectively. The adsorption kinetics of phenol using NL and ACL followed pseudo-second-order model with high correlation coefficients. In addition, the diffusion mechanism study indicated that the film diffusion had significant influence on the sorption rate-limiting step for both adsorbents. According to thermodynamic study, the adsorption operation was nonspontaneous, exothermic and primarily physical in nature. This study summed up treatment of two environmental issues. In one hand, recovery of solid agro-waste (date palm leaf) and in the other hand, treatment of polluted water by low-cost adsorbents.

Acknowledgments

The authors would like to thank the staff of Sahara Geology Laboratory and Scientific and Technical Research Centre for Physical and Chemical Analysis, for their valuable cooperation in the experimental tests achievement.

Data availability statement

The data that support the findings of this study are available from the corresponding author, [Abderrahim KHELFAOUI], upon reasonable request.

Disclosure statement

The authors reported no potential conflict of interest.

References

[1] A. Ahmadi, R. Foroutan, H. Esmaeili, S.J. Peighambardoust, S. Hemmati, B. Ramavandi, Montmorillonite clay/starch/$CoFe_2O_4$ nanocomposite as a superior functional material for uptake of cationic dye molecules from water and wastewater, Mater. Chem. Phys., 284 (2022) 126088, doi: 10.1016/j.matchemphys.2022.126088.

[2] W.W. Anku, M.A. Mamo, P.P. Govender, Phenolic Compounds in Water: Sources, Reactivity, Toxicity and Treatment Methods, M. Soto-Hernandez, M. Palma-Tenango, M. del Rosario Garcia-Mateos, Eds., Phenolic Compounds—Natural Sources, Importance and Applications, InTechOpen, 2017, pp. 420–443.

[3] W. Raza, J. Lee, N. Raza, Y. Luo, K.H. Kim, J. Yang, Removal of phenolic compounds from industrial wastewater based on membrane-based technologies, J. Ind. Eng. Chem., 71 (2019) 1–18.

[4] Z. Asadgol, H. Forootanfar, S. Rezaei, A.H. Mahvi, M.A. Faramarzi, Removal of phenol and bisphenol—a catalyzed by laccase in aqueous solution, J. Environ. Health Sci. Eng., 12 (2014) 1–5.

[5] J. Michałowicz, W. Duda, Phenols – sources and toxicity, Pol. J. Environ. Stud., 16 (2007) 347–362.

[6] A.Q. Jaradat, A.R. Shtayat, S. Odat, A coagulation–flocculation process combined with continuous adsorption using eggshell waste materials for phenols and PAHs removal from landfill leachate, Environ. Eng. Res., 27 (2022) 210133, doi: 10.4491/eer.2021.133.

[7] M. Schwarze, S. Borchardt, M.L. Frisch, J. Collis, C. Walter, P.W. Menezes, P. Strasser, M. Driess, M. Tasbihi, Degradation of phenol via an advanced oxidation process (AOP) with immobilized commercial titanium dioxide (TIO_2) photocatalysts, Nanomater, 13 (2023) 1249, doi: 10.3390/nano13071249.

[8] A. Almasi, M. Mahmoudi, M. Mohammadi, A. Dargahi, H. Biglari, Optimizing biological treatment of petroleum industry wastewater in a facultative stabilization pond for simultaneous removal of carbon and phenol, Toxin Rev., 40 (2019) 189–197.

[9] M. Wawrzkiewicz, A. Wołowicz, Z. Hubicki, Strongly basic anion exchange resin based on a cross-linked polyacrylate for simultaneous C.I. Acid Green 16, Zn(II), Cu(II), Ni(II) and phenol removal, Molecules, 27 (2022) 2096, doi: 10.3390/molecules27072096.

[10] M. Zamouche, M. Chermat, Z. Kermiche, H. Tahraoui, M. Kebir, J.C. Bollinger, A. Amrane, L. Mouni, Predictive model based on k-nearest neighbour coupled with the gray wolf optimizer algorithm (KNN_GWO) for estimating the amount of phenol adsorption on powdered activated carbon, Water, 15 (2023) 493, doi: 10.3390/w15030493.

[11] G. Issabayeva, S.Y. Hang, M.C. Wong, M.K. Aroua, A review on the adsorption of phenols from wastewater onto diverse groups of adsorbents, Rev. Chem. Eng., 34 (2017) 855–873.

[12] R. Foroutan, S.J. Peighambardoust, R. Mohammadi, S.H. Peighambardoust, B. Ramavandi, Development of new magnetic adsorbent of walnut shell ash/starch/Fe_3O_4 for effective copper ions removal: treatment of groundwater samples, Chemosphere, 296 (2022) 133978, doi: 10.1016/j.chemosphere.2022.133978.
[13] S. Ho, Low-cost adsorbents for the removal of phenol/phenolics, pesticides, and dyes from wastewater systems: a review, Water, 14 (2022) 3203.
[14] Md. Ahmaruzzaman, Adsorption of phenolic compounds on low-cost adsorbents: a review, Adv. Colloid Interface Sci., 143 (2008) 48–67.
[15] B.H. Hameed, A.A. Rahman, Removal of phenol from aqueous solutions by adsorption onto activated carbon prepared from biomass material, J. Hazard. Mater., 160 (2008) 576–581.
[16] A. Ahmad, S.A. Naqvi, M.J. Jaskani, M. Waseem, E. Ali, I.A. Khan, M. Faisal Manzoor, A. Siddeeg, R.M. Aadil, Efficient utilization of date palm waste for the bioethanol production through Saccharomyces cerevisiae strain, Food Sci. Nutr., 9 (2021) 2066–2074.
[17] A. Faiad, M. Alsmari, M.M.Z. Ahmed, M.L. Bouazizi, B. Alzahrani, H. Alrobei, Date palm tree waste recycling: treatment and processing for potential engineering applications, Sustainability, 14 (2022) 1134, doi: 10.3390/su14031134.
[18] S.E. Agarry, O.A. Aworanti, Kinetics, isothermal and thermodynamic modelling studies of hexavalent chromium ions adsorption from simulated wastewater onto parkia biglobosa-sawdust derived acid-steam activated carbon, Appl. J. Environ. Eng., 3 (2017) 58–76.
[19] P. Maziarka, P. Sommersacher, X. Wang, N. Kienzl, S. Retschitzegger, W. Prins, N. Hedin, F. Ronsse, Tailoring of the pore structures of wood pyrolysis chars for potential use in energy storage applications, Appl. Energy, 286 (2021) 116431, doi: 10.1016/j.apenergy.2020.116431.
[20] M.M. Nabeel Aljumaili, Y.I. Abdul-Aziz, High surface area peat moss biochar and its potential for chromium metal adsorption from aqueous solutions, S. Afr. J. Chem. Eng., 46 (2023) 22–34.
[21] Y. Önal, C. Akmil-Başar, Ç. Sarıcı-Özdemir, S. Erdoğan, Textural development of sugar beet bagasse activated with $ZnCl_2$, J. Hazard. Mater., 142 (2007) 138–143.
[22] A. Machrouhi, H. Alilou, M. Farnane, S. El Hamidi, M. Sadiq, M. Abdennouri, H. Tounsadi, N. Barka, Statistical optimization of activated carbon from *Thapsia transtagana* stems and dyes removal efficiency using central composite design, J. Sci. Adv. Mater. Dev., 4 (2019) 544–553.
[23] M. Ding, C. Li, F. Chen, Isolation and characterization of cellulose nanocrystals from cloth hairs and evaluation of their compatibility with PLLA, Cellulose, 24 (2017) 4785–4792.
[24] G. Rajeshkumar, V. Hariharan, G.L. Devnani, J. Prakash Maran, M.R. Sanjay, S. Siengchin, N.A. Al-Dhabi, K. Ponmurugan, Cellulose fiber from date palm petioles as potential reinforcement for polymer composites: physicochemical and structural properties, Polym. Compos., 42 (2021) 3943–3953.
[25] Z. Ma, Y. Yang, Y. Wu, J. Xu, H. Peng, X. Liu, W. Zhang, S. Wang, In-depth comparison of the physicochemical characteristics of bio-char derived from biomass pseudo components: hemicellulose, cellulose, and lignin, J. Anal. Appl. Pyrolysis, 140 (2019) 195–204.
[26] S. Darmawan, N.J. Wistara, G. Pari, A. Maddu, W. Syafii, Characterization of lignocellulosic biomass as raw material for the production of porous carbon-based materials, BioRes, 11 (2016) 3561–3574.
[27] I. Ben Salem, M. El Gamal, M. Sharma, S. Hameedi, F.M. Howari, Utilization of the UAE date palm leaf biochar in carbon dioxide capture and sequestration processes, J. Environ. Manage., 299 (2021) 113644, doi: 10.1016/j.jenvman.2021.113644.
[28] M.S. Shamsuddin, N.R.N. Yusoff, M.A. Sulaiman, Synthesis and characterization of activated carbon produced from kenaf core fiber using H_3PO_4 activation, Procedia Chem., 19 (2016) 558–565.
[29] A. Sukoyo, G. Djoyowasito, Y. Wibisono, Unravelling the potency of activated carbon powder derived from cultivated marine microalgae as a promising filler in mixed matrix membranes, AgriEngineering, 1 (2019) 188–204.
[30] S. You, Y.S. Ok, S.S. Chen, D.C.W. Tsang, E.E. Kwon, J. Lee, C.-H. Wang, A critical review on sustainable biochar system through gasification: energy and environmental applications, Bioresour. Technol., 246 (2017) 242–253.
[31] S. Bousba, A.H. Meniai, Removal of phenol from water by adsorption onto sewage sludge-based adsorbent, Chem. Eng. Trans., 40 (2014) 235–240.
[32] M. Jain, S.A. Khan, A. Sahoo, P. Dubey, K.K. Pant, Z.M. Ziora, M.A.T. Blaskovich, Statistical evaluation of cow-dung derived activated biochar for phenol adsorption: adsorption isotherms, kinetics, and thermodynamic studies, Bioresour. Technol., 352 (2022) 127030, doi: 10.1016/j.biortech.2022.127030.
[33] S. Mishra, S.S. Yadav, S. Rawat, J. Singh, J.R. Koduru, Corn husk derived magnetized activated carbon for the removal of phenol and para-nitrophenol from aqueous solution: interaction mechanism, insights on adsorbent characteristics, and isothermal, kinetic and thermodynamic properties, J. Environ. Manage., 246 (2019) 362–373.
[34] M. Mushtaq, H.N. Bhatti, M. Iqbal, S. Noreen, Eriobotrya japonica seed biocomposite efficiency for copper adsorption: isotherms, kinetics, thermodynamic and desorption studies, J. Environ. Manage., 176 (2016) 21–33.
[35] G. Nirmala, T. Murugesan, K. Rambabu, K. Sathiyanarayanan, P.L. Show, Adsorptive removal of phenol using banyan root activated carbon, Chem. Eng. Commun., 208 (2019) 831–842.
[36] A. Mandal, P. Mukhopadhyay, S.K. Das, Adsorptive removal of phenol from wastewater using guava tree bark, Environ. Sci. Pollut. Res., 27 (2020) 23937–23949.
[37] A.A.A. Darwish, M. Rashad, H.A. AL-Aoh, Methyl orange adsorption comparison on nanoparticles: isotherm, kinetics, and thermodynamic studies, Dyes Pigm., 160 (2019) 563–571.
[38] S. Alafnan, A. Awotunde, G. Glatz, S. Adjei, I. Alrumaih, A. Gowida, Langmuir adsorption isotherm in unconventional resources: applicability and limitations, J. Pet. Sci. Eng., 207 (2021) 109172, doi: 10.1016/j.petrol.2021.109172.
[39] J. Wang, X. Guo, Adsorption isotherm models: classification, physical meaning, application and solving method, Chemosphere, 258 (2020) 127279, doi: 10.1016/j.chemosphere.2020.127279.
[40] N. Ayawei, A.N. Ebelegi, D. Wankasi, Modelling and interpretation of adsorption isotherms, J. Chem., 2017 (2017) 1–11.
[41] L. Liu, X.B. Luo, L. Ding, S.L. Luo, Chapter 4 - Application of Nanotechnology in the Removal of Heavy Metal From Water, X. Luo, F. Deng, Eds., Nanomaterials for the Removal of Pollutants and Resource Reutilization: Micro and Nano Technologies, Elsevier, Amsterdam, 2019, pp. 83–147.
[42] Q. Hu, Z. Zhang, Application of Dubinin–Radushkevich isotherm model at the solid/solution interface: a theoretical analysis, J. Mol. Liq., 277 (2019) 646–648.
[43] O. Laçin, F. Demir, B. Bastaban, Determined of equilibrium adsorption isotherm model pertechnetate oxoanion onto activated carbon, Sinop. Uni. J. Nat. Sci., 4 (2019) 37–46.
[44] A.D. Zand, M.R. Abyaneh, Adsorption of lead, manganese, and copper onto biochar in landfill leachate: implication of non-linear regression analysis, Sustain. Environ. Res., 30 (2020) 1–16.
[45] K. Noufel, N. Djebri, N. Boukhalfa, M. Boutahala, A. Dakhouche, Removal of bisphenol A and trichlorophenol from aqueous solutions by adsorption with organically modified bentonite, activated carbon composites: a comparative study in single and binary systems, Groundwater Sustainable Dev., 11 (2020) 100477, doi: 10.1016/j.gsd.2020.100477.
[46] Z.H. Ho, L.A. Adnan, Phenol removal from aqueous solution by adsorption technique using coconut shell activated carbon, Trop. Aqua. Soil Pollut., 1 (2021) 98–107.
[47] H. Cherifi, S. Hanini, F. Bentahar, Adsorption of phenol from wastewater using vegetal cords as a new adsorbent, Desalination, 244 (2009) 177–187.
[48] Z. Gong, S. Li, W. Han, J. Wang, J. Ma, X. Zhang, Recyclable graphene oxide grafted with poly(N-isopropylacrylamide) and

its enhanced selective adsorption for phenols, Appl. Surf. Sci., 362 (2016) 459–468.
[49] A. Gupta, C. Balomajumder, Simultaneous adsorption of Cr(VI) and phenol onto tea waste biomass from binary mixture: multicomponent adsorption, thermodynamic and kinetic study, J. Environ. Chem. Eng., 3 (2015) 785–796.
[50] M.A. Khan, A. Ahmad, Kinetics and thermodynamic studies of phenol adsorption on nanocomposite, Desal. Water Treat., 57 (2015) 11255–11265.
[51] O. Abdelwahab, N.K. Amin, Adsorption of phenol from aqueous solutions by *Luffa cylindrica* fibers: kinetics, isotherm, and thermodynamic studies, Egypt. J. Aquat. Res., 39 (2013) 215–223.
[52] J. Numbonui Ghogomu, D. Tsemo Noufame, E. Buleng Njoyim Tamungang, D. Ajifack, J. Nsami Ndi, J. Mbadcam Ketcha, Adsorption of phenol from aqueous solutions onto natural and thermally modified kaolinitic materials, Int. J. Biol. Chem. Sci., 8 (2015) 2325–2338.
[53] A. Mandal, S.K. Das, Phenol adsorption from wastewater using clarified sludge from basic oxygen furnace, J. Environ. Chem. Eng., 7 (2019) 103259, doi: 10.1016/j.jece.2019.103259.
[54] Y. Dehmani, T. Lamhasni, A. Mohsine, Y. Tahri, H.S. Lee, H. Lgaz, A.A. Alrashdi, S. Abouarnadasse, Adsorption removal of phenol by oak wood charcoal activated carbon, Biomass Convers. Biorefin., (2022), doi: 10.1007/s13399-022-03036-5.
[55] H.M. El-Bery, M. Saleh, R.A. El-Gendy, M.R. Saleh, S.M. Thabet, High adsorption capacity of phenol and methylene blue using activated carbon derived from lignocellulosic agriculture wastes, Sci. Rep., 12 (2022) 5499, doi: 10.1038/s41598-022-09475-4.
[56] E.H. Gürkan, R.B. Akyol, S. Çoruh, Kinetic, isotherm modelling analyses of the adsorption of phenol on activated carbon/alginate composites, Int. J. Phytorem., 25 (2023) 832–839.
[57] T.R. Sahoo, B. Prélot, Adsorption Processes for the Removal of Contaminants from Wastewater: The Perspective Role of Nanomaterials and Nanotechnology, B. Bonelli, F. Freyria, I. Rossetti, R. Sethi, Eds., Nanomaterials for the Detection and Removal of Wastewater Pollutants: Micro and Nano Technologies, Elsevier, Amsterdam, 2020, pp. 161–222.
[58] R.M.C. Viegas, M. Campinas, H. Costa, M. João Rosa, How do the HSDM and Boyd's model compare for estimating intraparticle diffusion coefficients in adsorption processes, Adsorption, 20 (2014) 737–746.
[59] M. Wakkel, B. Khiari, F. Zagrouba, Textile wastewater treatment by agro-industrial waste: equilibrium modelling, thermodynamics and mass transfer mechanisms of cationic dyes adsorption onto low-cost lignocellulosic adsorbent, J. Taiwan Inst. Chem. Eng., 96 (2019) 439–452.
[60] L. Fu, J. Li, G. Wang, Y. Luan, W. Dai, Adsorption behavior of organic pollutants on microplastics, Ecotoxicol. Environ. Saf., 217 (2021) 112207, doi: 10.1016/j.ecoenv.2021.112207.
[61] R. Foroutan, S.J. Peighambardoust, S. Ghojavand, S. Farjadfard, B. Ramavandi, Cadmium elimination from wastewater using potato peel biochar modified by ZIF-8 and magnetic nanoparticle, Colloid Interface Sci. Commun., 55 (2023) 100723, doi: 10.1016/j.colcom.2023.100723.
[62] D. Naidu, P. Pattanaik, A.A. Das, N.K Sahoo, Kinetic of phenol adsorption by mesoporous MCM-41 nanoparticles, Int. J. Innovative Technol. Exploring Eng. (IJITEE), 8 (2019) 316–323.
[63] X. Sun, L. Ma, G. Ye, L. Wu, J. Li, H. Xu, G. Huang, Phenol adsorption kinetics and isotherms on coal: effect of particle size, Energy Sources Part A, 43 (2019) 461–474.
[64] N.G. Rincón-Silva, J.C. Moreno-Piraján, L. Giraldo, Equilibrium, kinetics and thermodynamics study of phenols adsorption onto activated carbon obtained from lignocellulosic material (*Eucalyptus Globulus labill* seed), Adsorption, 22 (2015) 33–48.
[65] D.C.S. Alves, J.O. Gonçalves, B.B. Coseglio, T.A.L. Burgo, G.L. Dotto, L.A.A. Pinto, T.R.S. Cadaval, Adsorption of phenol onto chitosan hydrogel scaffold modified with carbon nanotubes, J. Environ. Chem. Eng., 7 (2019) 103460, doi: 10.1016/j.jece.2019.103460.
[66] W.P. Cheng, W. Gao, X. Cui, J.H. Ma, R.F. Li, Phenol adsorption equilibrium and kinetics on zeolite X/activated carbon composite, J. Taiwan Inst. Chem. Eng., 62 (2016) 192–198.
[67] M. Horsfall Jnr, A.I. Spiff, Effects of temperature on the sorption of Pb^{2+} and Cd^{2+} from aqueous solution by *Caladium bicolor* (Wild Cocoyam) biomass, Electron. J. Biotechnol., 8 (2005) 162–169.
[68] M. Salari, M.H. Dehghani, A. Azari, M.D. Motevalli, A. Shabanloo, I. Ali, High performance removal of phenol from aqueous solution by magnetic chitosan based on response surface methodology and genetic algorithm, J. Mol. Liq., 285 (2019) 146–157.
[69] N. Yadav, D. Narayan Maddheshiaya, S. Rawat, J. Singh, Adsorption and equilibrium studies of phenol and para-nitrophenol by magnetic activated carbon synthesised from cauliflower waste, Environ. Eng. Res., 25 (2020) 742–752.
[70] A. Khelfaoui, N. Chaouch, Comparative adsorption study of phenol removal using *Phoenix dactylifera* fiber and its chemically activated carbon, Desal. Water Treat., 278 (2022) 182–194.
[71] X. Kong, H. Gao, X. Song, Y. Deng, Y. Zhang, Adsorption of phenol on porous carbon from *Toona sinensis* leaves and its mechanism, Chem. Phys. Lett., 739 (2020) 137046, doi: 10.1016/j.cplett.2019.137046.
[72] N. Mojoudi, N. Mirghaffari, M. Soleimani, H. Shariatmadari, C. Belver, J. Bedia, Phenol adsorption on high microporous activated carbons prepared from oily sludge: equilibrium, kinetic and thermodynamic studies, Sci. Rep., 9 (2019) 19352, doi: 10.1038/s41598-019-55794-4.
[73] D. Zhang, P. Huo, W. Liu, Behavior of phenol adsorption on thermal modified activated carbon, Chin. J. Chem. Eng., 24 (2016) 446–452.
[74] B. Xie, J. Qin, S. Wang, X. Li, H. Sun, W. Chen, Adsorption of phenol on commercial activated carbons: modelling and interpretation, Int. J. Environ. Res. Public Health, 17 (2020) 789, doi: 10.3390/ijerph17030789.